



Clinical validation of an automatic system to categorize tear film lipid layer patterns

M J Giráldez, C García-Resúa, H Pena-Verdeal, J Garcia-Queiruga, and E Yebra-Pimentel

Department of Applied Physics (Optometry Area), Universidade de Santiago de Compostela, Spain

Dedicated to Prof Jay M Enoch

This paper deals with validation of clinical performance of the objective application *iDEAS* (Dry Eye Assessment System) to categorize different zones of tear film lipid layer patterns (LLPs). All procedures followed the Declaration of Helsinki, and the protocol was reviewed and approved by the Ethics Committee of the University of Santiago de Compostela. The authors report no conflicts of interest and have no proprietary interest in any of the materials mentioned in this article. © Anita Publications. All rights reserved.

Keywords: Microsaccades, Preferential looking, Visual search, Latency, Priming, Eye movements.

1 Introduction

Dry eye disease (DED) is a multifactorial disease of the tear film with potential damage to the ocular surface [1]. As a multifactorial syndrome, DED is difficult to diagnose and several tests are needed [2]. However, despite a large number of tests are available to assess different features of the tear film, such as tear quality and quantity, most of them show high variation leading to poor to fair diagnostic repeatability [1]. In this sense, the lack of correlation between ocular symptoms and the results of many usual clinical tests for dry eye has been well reported [3-5]. Furthermore, there is a wide discrepancy in the epidemiology of DED, which is the result of the lack of consensus of which combination of tests should be used to define the disease, either in the clinic or for a research protocol [6]. Therefore, the main goal in current clinical research is to make clinical tests more objective [7-13] and to establish a strong diagnostic criterion for DED [6].

The “Dry Eye Workshop II” (DEWS-II) and the “The International Workshop on Meibomian Gland Dysfunction” [14,15] pointed out that the meibomian gland dysfunction (MGD) is the main cause of evaporative dry eye and may also have some association with aqueous-deficient dry eye. MGD is a chronic, diffuse abnormality of the meibomian glands, commonly characterized by terminal duct obstruction and/or qualitative/quantitative changes in glandular secretion [15-17]. It is important to note that the meibomian glands secrete the lipids that conform to the outer lipid layer of the tear film, which plays a major role in limiting evaporation during the inter-blink period, affecting tear film stability [18,19]. Therefore, lipid layer assessment is essential in dry eye evaluation.

Commonly, the lipid layer is evaluated by assessing its thickness (LLT); this parameter is an indicator of tear film quality and can be assessed by non-invasively imaging the superficial lipid layer by interferometry using an instrument such as the Tearscope-plus [20-23]. Guillon proposed five main grades

Corresponding author

e mail: mjesus.giraldez@usc.es (M J Giráldez)

of LLT interference patterns (based on texture and colour) for observations made using the Tearscope-plus [20]: open meshwork (OM), closed meshwork (CM), flow or wave (W), amorphous (AM) and colour fringe (CO). This author also described abnormal lipid layer patterns (LLPs). Although this method has been proven useful to evaluate the quality and structure of the tear film [20,24], it is affected by the subjective interpretation of the observer. Thicker lipid layers (≥ 90 nm) are readily observed since they produce colour and wave patterns. However, thin lipid layers (≤ 60 nm) are difficult to visualize, since colour fringes and other distinct morphological features are not present and their interpretation is more subjective [25]. Training also affects the interpretation of the LLPs and there is a learning curve for Tearscope tear interference pattern grading [26]. These drawbacks have led to the less use of this technique. Techniques developed to objectively calculate LLT are based on sophisticated optics systems [27] or assess LLT only according to interference colours observed using an interference camera [28]. Recently, the analysis of grey level intensity values in videokeratography was applied to assess - tear film (TF) behaviour as an alternative biomarker to objectively grade LLT [29].

Artificial intelligence (AI) based on machine learning and deep learning techniques is increasingly applied to healthcare in different specialties. In ophthalmology, AI has been primarily applied to image-based diagnosis of diabetic retinopathy, glaucoma, age-related macular degeneration and retinopathy of prematurity, most of which are retinal diseases [30]. Moreover, based on optical coherence tomography, slit-lamp images and even ordinary eye images, AI applied to eye evaluation achieve robust performance in the detection and management of ocular surface and tear film anomalies [31]. *iDEAS* application was previously developed to a more objective way to classify the LLPs provided by the Tearscope [32]. Although the Tearscope protocol is a useful tear film test, several technical aspects need to be addressed yet to improve its performance. LLP classification is difficult and requires training, such that a large bank of comprehensive images and detailed descriptions of each pattern would be useful in the development of new AI technology and would help observers distinguish between one pattern grade and the next. Moreover, LLPs are not always homogeneous, and a combination of patterns may appear. It is usually found that the lipid layer is thicker over the lower cornea and thinner in the central corneal area [25]. Thus, sometimes an LLP has to be classified as showing a combined (representing several lipid thicknesses) [20] rather than a single pattern. Using the previously developed tool *iDEAS* (Dry Eye Assessment System), an LLP can be categorized by zones and thus the heterogeneity of a pattern can also be graded [33,34].

Therefore, based on the objectives of the DEWS-II, the purpose of this study was to validate the performance of the automatic software application (*iDEAS*) to objectively categorize different zones of LLPs in one image.

2 Methods

The validation was done by comparing the zones of LLP categorization between 4 experienced observers and the automatic system *iDEAS*.

2.1. Subjects

Subjects were recruited among subjects who attended the Optometry Clinic for an eye examination. Subjects were excluded if they had an ocular infection or an ocular allergy, were contact lens users, taking a prescription eye medication, or were pregnant or breastfeeding. Subjects were asked not to wear eye makeup before the clinical protocol. The study protocol adhered to the tenets of the Declaration of Helsinki and was approved by the Ethics Committee of the Universidade de Santiago de Compostela (Spain).

2.2. Equipment and image/video acquisition procedure

Tear film lipid layer was examined using a Tearscope-plus® (Keeler, Windsor, UK). This instrument, designed by Guillon, is the instrument most commonly used in clinical practice for the rapid assessment of LLT and has been described in detail elsewhere [20].

2.2.1. Interference phenomena. Interpretation of the observations

When observing the appearance of the lipid layer by interference phenomena it can be appreciated seen the presence of interference fringes. To observe interference phenomena, it is necessary to use coherent light sources, i.e., sources whose phase difference remains constant in time. A simple manner in which this can be accomplished is by using a single light source and its optical image [35]. To observe interference phenomena, it is necessary to use coherent light sources, i.e., sources whose phase difference remains constant in time. A simple manner in which this can be accomplished is by using a single light source and its optical image [35].

In the case of the tear film, there are two interfering beams; the beam reflected from the air-lipid interface of the tear film, and the beam reflected from the lipid-aqueous interface of the tear film.[36]. The two beams originate from the same point of the single light source and, in fact, are two images of it, so the beams satisfy the requirement of coherence. Figure 1 shows the scheme of this phenomenon between two flat boundaries, air-lipid boundary and lipid-aqueous boundary and follows the expression [35].

$$m(d, \phi', \lambda) = \frac{2n(\lambda)d \cos(\phi')}{\lambda}$$

where d is the distance between both boundaries (LLP thickness), m is the order of interference, λ is the wavelength of light, $n(\lambda)$ is the refractive index that depends on wavelength and ϕ' is the angle of Refraction, which is normal to corneal surface.

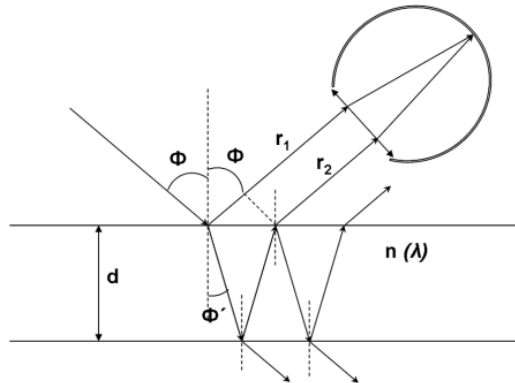


Fig 1. Optical diagram which shows the interference. r_1 is light beam reflected from the air-lipid interface of the tear film, and r_2 is light beam reflected from the lipid-aqueous interface of the tear film. Both light beams r_1 and r_2 are originated from the same source. The thickness of the surface d generates an optical path difference between them and will produce interference fringes after recombination. ϕ is the incidence angle which is equal to reflected angle, whereas ϕ' is the refracted angle. $n(\lambda)$ is the refractive index, that depends on light wave length.

This interference phenomena can be visible by specular reflection, and the observer can appreciate an interference pattern (formed by fringes and/or colours) commonly known as tear film lipid layer pattern [20,36]. Colour fringes are related to LLT, so the determination of LLT can be extrapolated. However, the lipidic reflection does not always show a colour pattern. The observation of a colourless pattern (grey colour) is because its thickness is below the minimum thickness to produce interference fringes. Korb [25] established the LLT that corresponded to each colour.

2.2.2. Image Acquisition

Image acquisition was performed as done elsewhere [33]. The Tearscope was attached to a Topcon SL-D4 slit-lamp using an R900 Goldmann tonometer support. The biomicroscope magnification was set at 16 \times and illumination was provided by the Tearscope.

To ensure that there is no variation in the size of the observation area during the acquisition procedure, the Tearscope was fixed to the slit-lamp such that the distance between the chin rest and instrument remain constant during the imaging procedure. To centre the lipid layer region of interest (ROI), subjects were instructed to fix their sight on a target.

Interference images of the lipid layer were captured by a Topcon DV-3 digital camera and stored via Topcon IMAGEnet i-base at a spatial resolution of 1024×768 pixels in the RGB colour space. Because the tear film is not static between blinks, a video was recorded and the best image for processing was selected. All images were then uploaded to the database included in the iDEAS software for image classification. Around 2000 images were uploaded in the iDEAS database at the time of the study. Then, a set of images that better fulfilled the quality requirements (free of blur, lipid layer well spread after a complete blink and well centered) was selected. This yielded 50 images that were used for our study.

2.3 iDEAS

iDEAS (Dry Eye Assessment System) is a web application designed to join several services in the field of optical image processing [37]. Technical features and a wide description of iDEAS application have been previously indicated [34].

Regarding image tools, the application classifies the tear film image and assigns a specific LLP type to the whole image. This automatic classification tool has been proposed elsewhere [38,39], and was properly validated by optometrists by comparing LLP classifications of 105 images with those provided by 3 observers [33]. The process consists of detecting the ROI of the image; extracting its colour, texture features; generating a vector that describes it, and finally classifying it into one of the target categories. It should be highlighted that this process provides unbiased results with maximum accuracy over 97% and processing time under 1 second [32], which saves time for experts. In clinical terms, the results revealed that this tool was able to classify LLPs as subjective observers.

On the other hand, the web application allows users to manually trace different regions associated with a specific LLP. This determines that an image of several discrete LLP zones can be subjectively categorized in one image.

An automatic tool based on techniques for colour and texture analysis [39] was previously developed to identify different LLP patterns in a single patient image [40]. However, it used the unreal background category, which represents the areas of the images in which there is no LLP. Since tear film lipid layer images have a great level of variability, as they cannot be characterized by uniform texture features, the accuracy of the classifier may be affected [40]. Thus, the method proposed here consists of a weighted voting system that considers the class-membership probabilities provided by a soft classifier and uses a minimum threshold to distinguish the background from the Guillon categories without using any unreal category. The research methodology proposed to create tear film maps based on the lipid interference patterns consists of five stages (Fig 2).



Fig 2. Scheme of the research methodology to create tear films maps.

The input data is a tear film image acquired with the Tearscope-plus, and the output data is a labelled image based on the interference patterns defined by Guillon. Firstly, the region of interest, in which the further analysis will take place, is located. Next, each local window inside it is analysed in terms of colour and texture features, and its class-membership probabilities are calculated by using a soft classifier. Following, the segmentation is performed using the weight voting system in such a way that every pixel

of every window receives a vote associated to each lipid layer classification

$$v_c = w_1 \cdot p_c + w_2 \cdot p_c/d,$$

where p_c is the probability of belonging to the class c , d is the distance from the pixel to the centre of the window, and w_1 and w_2 are weight the probability and the distance, respectively. As windows are overlapped, each pixel belongs to several categories and so the votes received from each category are added up. Thus, the pixel is assigned to the most voted category only if its total number of votes is greater than a threshold. Finally, the tear film map obtained is post-processed to eliminate the small regions which usually correspond to false positives or noisy areas.

2.3.1 Characterization of the lipid layer patterns.

Both image tools available in the *i*DEAS web system are based on the characterization of the lipid layer patterns by means of colour and texture information. Broadly speaking, colour and interference patterns are the two discriminant features of the Guillon categories for lipid layer assessment. On the one hand, some categories show distinctive colour characteristics which motivate the colour analysis step. On the other hand, the interference phenomena can be characterized as a textured pattern, since thicker lipid layers show defined patterns while thinner layers are more homogeneous.

For colour analysis, the use of the Lab colour space is considered according to previous research [39]. The CIE 1976 L*a*b colour space [41] (Lab) is a chromatic colour space that describes all the colours which the human eye can perceive. It was defined by the International Commission on Illumination, abbreviated as CIE from its French title Commission Internationale de l'Eclairage. The Lab is a 3D model where its three coordinates represent: the luminance of the colour L, its position between magenta and green a, and its position between yellow and blue b. Its use is recommended by CIE in images with natural illumination. In addition, this colour space is perceptually uniform, a very important characteristic since expert's perception is trying to be imitated. The use of the Lab colour space entails converting the three channels of the Tearscope image in RGB into the three components of Lab, which will be subsequently analysed in terms of texture.

Regarding texture analysis, the co-occurrence features technique is applied due to its effectiveness to characterize the LLPs [39]. Co-occurrence features [42] allow defining a texture descriptor based on the computation of the conditional joint probabilities of all pairwise combinations of grey levels, given an interpixel distance and an orientation. The method generates a set of grey level co-occurrence matrices (GLCM) and extracts several statistical measures from their elements. The Chebyshev distance is considered here and, in general, the number of matrices for a distance d is $4d$. From each GLCM, a set of 14 statistical measures proposed by Haralick *et al* [42] are computed, which represent features such as contrast or homogeneity. Finally, the mean and the range of these 14 statistics are calculated across matrices and a set of 28 features composes the texture descriptor for a particular distance.

2.4. Pattern classifications. Agreement among 4 experienced observers' methodology

Four experienced observers in LLP grading were asked to categorize the LLPs found in 50 images selected as described above. In each image, the observer marked the LLP zones of interest using the *i*DEAS tool (Fig 3a). The *i*DEAS program was then used to extract the zones for which there was agreement among all 4 observers (Fig 3b). These areas classified by observers were catalogued as "correct images" to be included in the database created to guide automatic LLP categorization.

Before the 4 observers started to categorize the LLPs, a set of example images of LLPs and instructions were presented to the experienced observers to improve pattern categorization (Guidance to subjective categorization of LLPs is depicted in the Appendix).

2.5. Data and statistical analysis

To validate this new application, the automatic LLP categorization was compared with that made by four experienced observers. In this manner, the areas marked by a reference observer, including automatic

system, were compared with the areas annotated by the others. That is, the number of pixels of the reference observer which match with other observers is added up and graphically represented. Therefore, if the reference observer LLP classification is compared with the rest of the observers, there are several pixels in which the reference observer agrees with 0, 1, 2, 3 or 4 observers. This comparison between experts was performed in such a way that each observer is used as the reference observer once, and so a total of five comparisons are obtained.

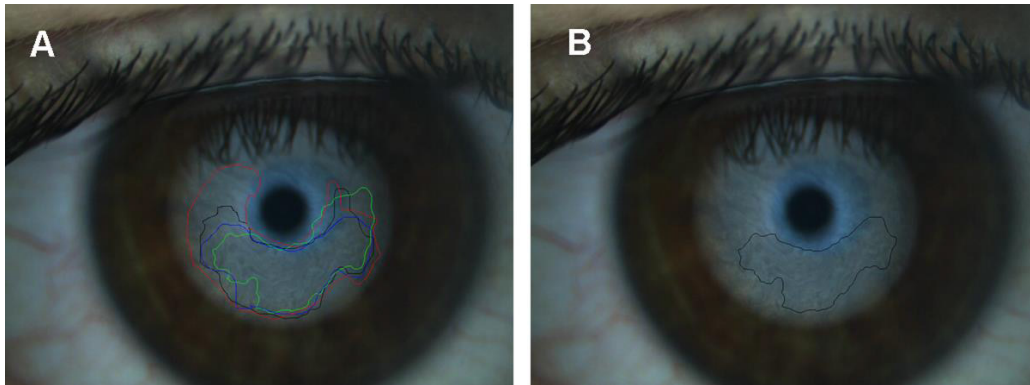


Fig 3. Image interpretation by 4 observers using the *iDEAS*. A) Overlapping zones marked by the observers; each color indicates the zone categorized by one observer. B) Zone for which there was an agreement among 4 observers. This zone was used as the reference image for the LLP descriptions provided in the main text (Results).

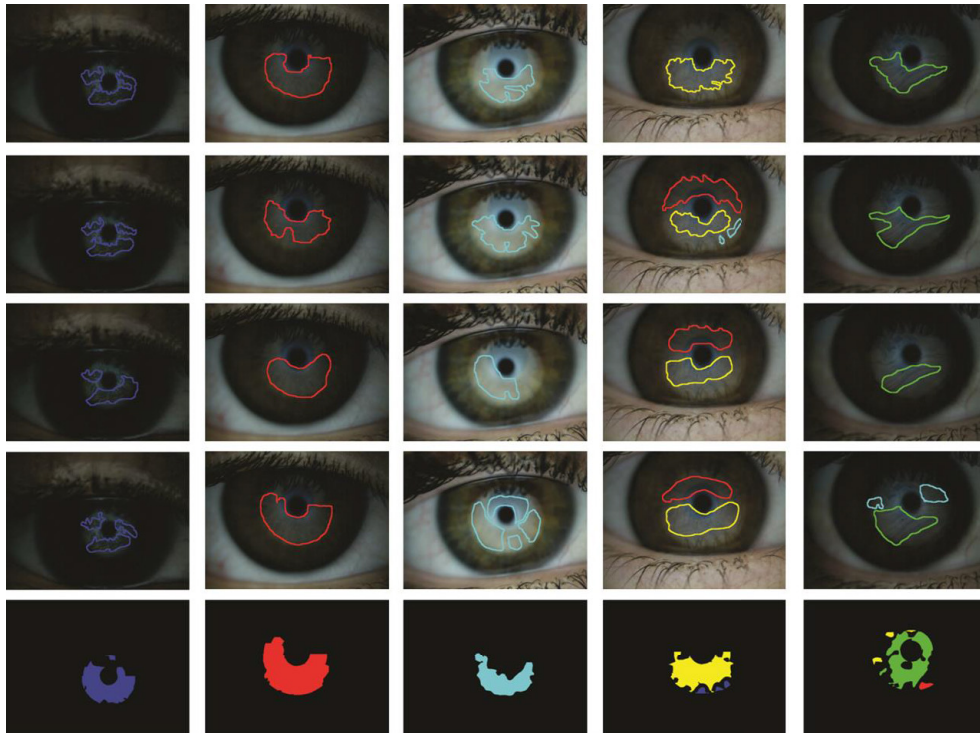


Fig 4. Annotations made by the 4 observers over 5 representative images, and their respective output images provided by the automatic system.

As an example, Fig 4 illustrates the annotations made by the 4 observers over 5 representative images and their respective output images provided by the automatic system. As can be seen, there are areas of the images in which the observers agree with the LLP, whereas there are other areas in which there is no agreement. The same situation can be appreciated if the output images are compared with the observers' annotations. Then, it was obtained the amount of LLP areas (counted in pixels) that each observer and *i*DEAS matched with the remaining ones. Finally, to perform statistical analysis feasibly, only two matches were considered for each reference observer as follows:

- Erroneous categorization (EC): It means those pixels that reference observer agreed with 0 observers or were marked only by the reference observer.
- Perfect categorization (PC): That means PC represents those pixels which are in agreement with all the observers.

Kolmogorov-Smirnov test was done for each variable, and it was found that they did not follow a normal distribution ($p < 0.05$), so nonparametric statistics was used.

To perform multiple comparisons a Kruskal-Wallis test was used. Finally, to perform pairwise comparisons, the Friedman test was used for independent variables, whereas a Wilcoxon test was used for dependent variables.

3 Results

50 images captured using the Tearscope were used. After examining all 50 images, 110 areas were assigned by all four observers to the same LLP category. Table 1 shows the LLPs detected.

Table 1. Number of zones on 50 images for which there was agreement among the 4 observers.

	Open Meshwork	Closed Meshwork	Wave	Amorphous	Color fringe
Zones indicated	25	22	20	26	17

Figure 5 shows the agreement in LLP categorization among observers (4 experienced observers and automatic system). In each comparison one of them was used as reference observer, thus observer 1, observer 2, observer 3, observer 4 and the automatic system are represented as reference observer in Fig 5 (A to E), respectively. Each figure shows in bar graphs number of pixels of the reference observer which match with other observers for each pattern. Note that the agreement between the categorization made by each observer and the remaining 4 is the same for each one. This was not the same when analysing the agreement between reference observer with experienced observers 0, 1, 2 and 3, respectively. If we focus our attention on the plot "system vs. all" (Fig 5E), it can be seen that there are little number of pixels that match with 0, 1, 2, and 3 observers. This fact means that the system has a conservative behaviour. In contrast, the graph "observer 3 vs. all" (Fig 5C) shows how observer 3 has a completely different behaviour since it tends to mark bigger regions.

The other three observers are in the middle of both extremes according to their respective graphs, which show a similar plot tendency. On the other hand, the system produces some output images which contain regions associated with the W pattern that does not match with any observer, and observer 3 annotated some areas associated with the CO pattern that does not match with any observer. Thus, not only does this anomalous behaviour appear in the images obtained by the system, but also in some of the ones annotated by the observers. Consequently, it could be said that the system behaves similar to the observers to a greater or lesser degree depending on the specific LLP.

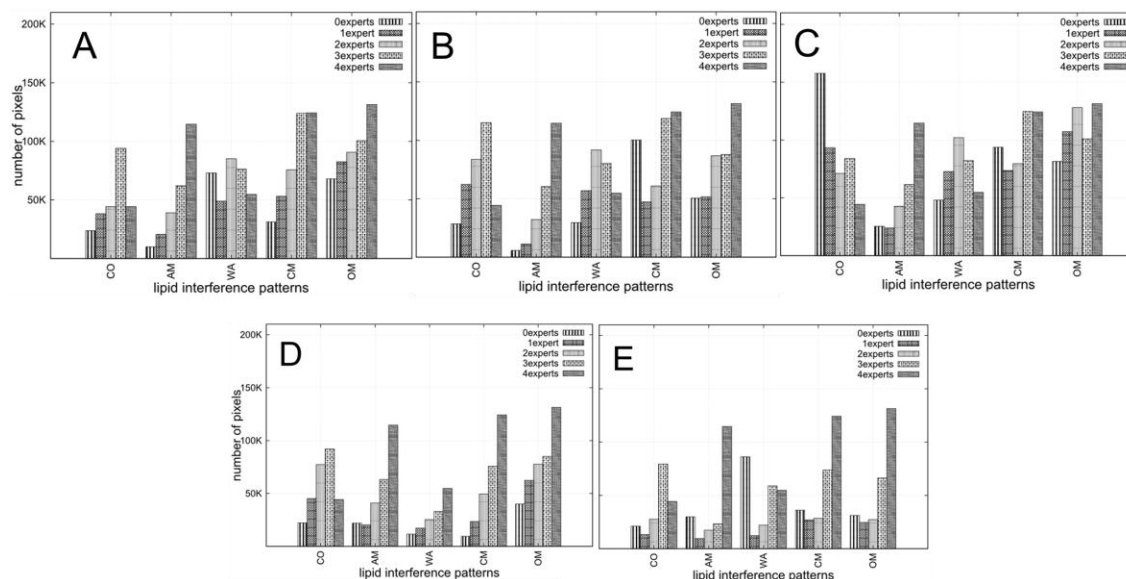


Fig 5. Bar graphs obtained by performing the comparison among the 5 observers (4 experienced observers and the automatic system). One observer is termed "reference observer" and is compared between the rest of the observers. In each comparison, the number of pixels of the reference observer which match with other observers, are shown. A) Observer 1 as "reference observer". B) Observer 2 as "reference observer". C) Observer 3 as "reference observer". D) Observer 4 as "reference observer". E) Automatic System as "reference observer".

3.1. Statistical analysis

3.1.1. Analysis of the categorization between the types of lipid layer patterns

Table 2 shows the descriptive statistics of the size area for both EC and PC (number of pixels) for each pattern type irrespective of the observers.

Table 2. Descriptive statistics of size areas quantified in pixels and in percentage of area for each lipid layer pattern irrespective of observers. Median and interquartile range (IQ) are indicated. "Erroneous categorization" means those pixels which reference observer agreed with 0 observers or were marked only by the reference observer. "Perfect categorization" means those pixels in agreement between reference observer and the remaining 4 observers.

Median (IQ)	Number of pixels		Percentage of area	
	Erroneous categorization	Perfect categorization	Erroneous categorization	Perfect categorization
Open Meshwork	3245 (5539)	9861 (33908)	46.62 %	53.38 %
Closed Meshwork	2672 (4126)	16330 (15651)	22.59 %	77.41 %
Wave	3193 (4682)	5100 (12012)	52.35 %	47.65 %
Amorphous	1423 (3448)	12089 (9259)	20.36 %	79.63 %
Color fringe	3033 (6026)	4268 (33908)	55.14 %	44.86 %

Kruskal-Wallis test showed that there was not found statistical differences of size areas among the type of patterns for both EC ($p = 0.100$) and PC ($p = 0.080$). These results reveal that the 4 experienced observers and the automatic system categorized all LLPs in the same way, that is, neither type of LLP was categorized more erroneous than the remaining LLP.

Resulting from the methodology of this study, we provided a set of LLP images in accordance with 4 experienced observers that can be used as a guide for LLP classification. Figures 6 to 10 show an example of each type of LLP, in which the area indicated by a black line was similarly interpreted by the 4 observers. Thus, of the 110 LLPs defined, we provide 4 images (corresponding to four different patients) of the zones assigned to each LLP as a guide for pattern categorization. After examining the images, we detected the more characteristic features for each LLP that permitted us to enhance the description of the patterns implemented by Guillon [20]. This description is indicated in Table 3.

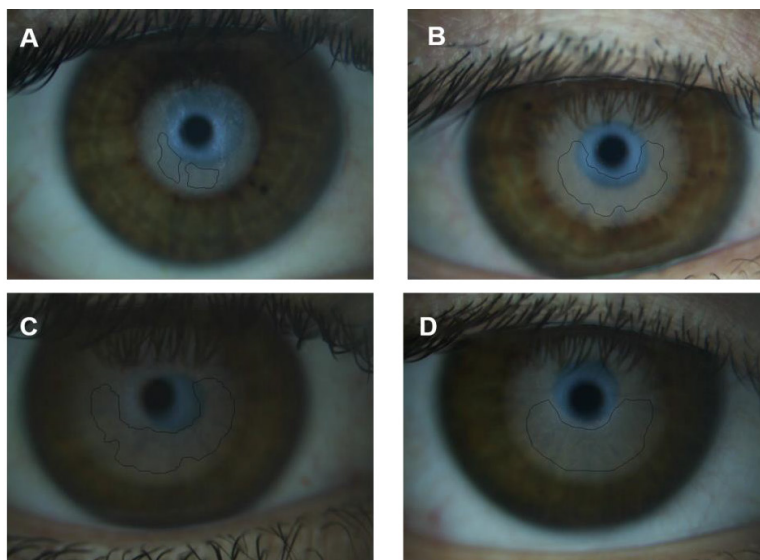


Fig 6. Matching zone identified by 4 observers as an open meshwork LLP. A-D images represents four different patients.

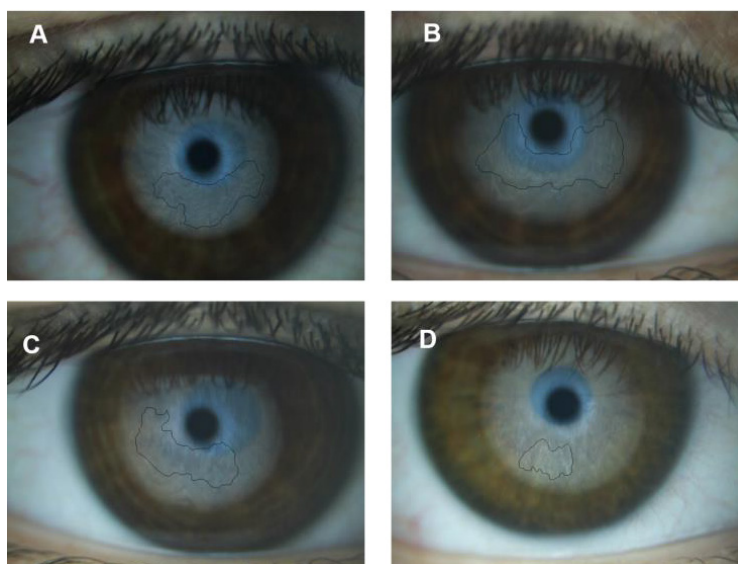


Fig 7. Matching zone identified by 4 observers as a closed meshwork LLP. A-D images represents four different patients.

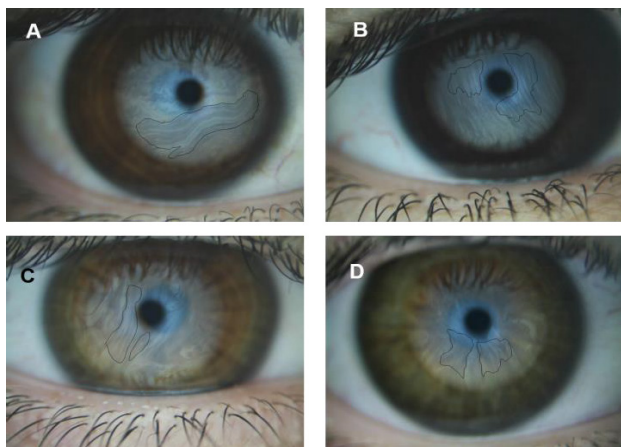


Fig 8. Matching zone identified by 4 observers as a wave LLP. A-D images represents four different patients.

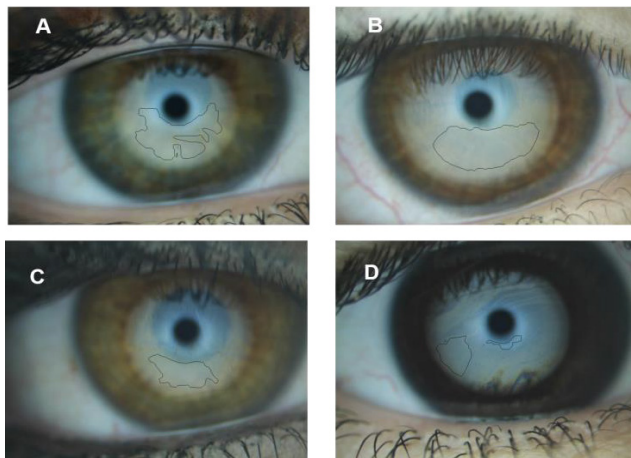


Fig 9. Matching zone identified by 4 observers as an amorphous LLP. A-D images represents four different patients.

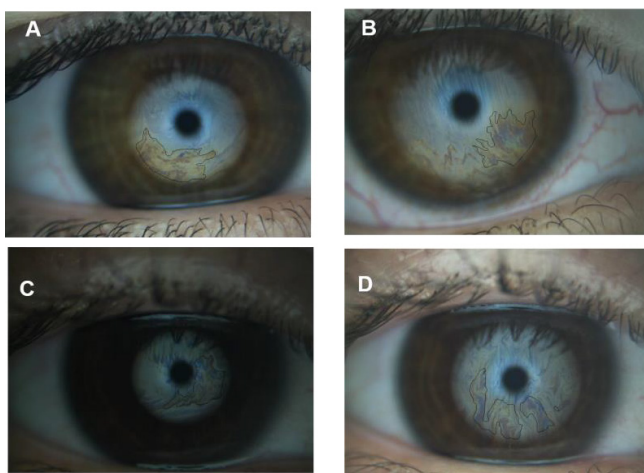


Fig 10. Matching zone identified by 4 observers as a color fringe LLP. A-D images represents four different patients.

Table 3. Description of the interpretation of each LLP that is derived from the categorization done by the observers and resulting from the zones in accordance with the four experienced observers. The areas in concordance were compiled by the software *iDEAS*. LLP: “lipid layer pattern”

LLP	Overview	Details considered when outlining the LLP
Open meshwork	This is the thinnest lipid layer visible and one of the most difficult to categorize	When outlining an OM zone with the <i>iDEAS</i> , bright areas should not be considered (these indicate an amorphous pattern). It should be noted that this pattern is barely visible, and the underlying iris will normally show through
Closed meshwork	This pattern reflects a thicker, more stable lipid layer than the OM, and its features are easier to detect	When marking a closed meshwork zone with the <i>iDEAS</i> , streaks appear larger, more marked and closer together than in the OM and OMCM; they may then join together to form large peaks or zigzags
Wave	This wavy pattern represents a stable tear film	When identifying zones of this pattern, we need to look for straight or almost straight, well-defined streaks.
Amorphous	This is the most homogeneous pattern	When outlining these zones with the <i>iDEAS</i> , we should bear in mind its lack of features and a non-visible iris (unlike in the OM pattern). Sometimes, it appears as a strictly amorphous pattern but with a few dispersed dark spots. Using the <i>iDEAS</i> , these spots should be avoided
Color fringe	Easiest LLP to categorize	We should consider that it is basically a set of colors (brown or yellow-brown colors appear first) on a yellow background. Thus, if we observe only a yellow color, we will consider it more an amorphous pattern

3.1.2. Comparison of the categorization between observers

Table 4 shows the descriptive statistics of the size of the EC area (number of pixels) for each observer irrespective of the LLP. The size of the PC area was not considered because PC means those pixels which are in agreement with the reference observer and the remaining 4 observers (**Table 2**), so all the five observers show the same value. Therefore, to compare the categorization among observers only EC was used, where the lower the size of the EC area, the better the performance of LLP categorization.

Table 4. Descriptive statistics of size areas (quantified in pixels) for each observer irrespective of lipid layer pattern. Median and interquartile range (IQ) are indicated. “Erroneous categorization” means those pixels that reference observer agreed with 0 observers or were marked only by the reference observer.

Number of pixels EC. Median (IQ)				
Observer 1	Observer 2	Observer 3	Observer 4	Automatic system
2416 (3773)	1829 (3617)	6354 (8282)	1509 (2841)	3360 (5015)

Statistical differences among observer’s categorization, including automatic system, were observed (Friedman test, $p < 0.001$). Wilcoxon test was used to check pair differences between observers (**Table 5**), and it was found that observer 3 showed a size of EC area significantly higher than by the remaining 4 observers ($p \leq 0.006$ for all comparisons, **Table 5**), indicating that observer 3 categorized worse than by the remaining observers. There was also a statistical difference between observer 4 and automatic system categorization ($p < 0.044$).

Table 5. Wilcoxon test outcomes. Pair wise comparisons between the amount of EC pixels categorized by two observers. In each comparison median of differences and level of statistical significance (p) are indicated. EC: “Erroneous categorization”, means those pixels that reference observer agreed with 0 observers or were marked only by the reference observer.

Pair wise comparisons. Lipid layer pattern categorization				
	Observer 1	Observer 2	Observer 3	Observer 4
Observer 1				
Observer 2	$p = 0.260$			
Observer 3	$p = 0.010$	$p = 0.006$		
Observer 4	$p = 0.090$	$p = 0.500$	$p < 0.001$	
Automatic system	$p = 0.550$	$p = 0.510$	$p = 0.003$	$p = 0.040$

Table 6 shows the descriptive statistics of the size of the EC area (number of pixels) categorized by each observer for each LLP. Friedman test showed that there were statistically significant differences among observers only for open meshwork LLP ($p = 0.020$), but that was not true for the remaining LLPs; closed meshwork ($p = 0.190$), wave ($p = 0.390$), amorphous ($p = 0.410$) and colour fringe ($p = 0.190$).

Table 6. Descriptive statistics of the size of the EC area (number of pixels) categorized by each observer for each LLP. Median and interquartile range (IQ) are indicated. EC: “Erroneous categorization”, means those pixels that reference observer agreed with 0 observers or were marked only by the reference observer

	Number of pixels EC. Median (IQ)				
	Observer 1	Observer 2	Observer 3	Observer 4	Automatic system
Open meshwork	4234 (9489)	1820 (5602)	10144 (8660)	1328 (2236)	5503 (4284)
Closed meshwork	3350 (5778)	2795 (3650)	4780 (16017)	1417 (2446)	4130 (4402)
Wave	2819 (1690)	1720 (3271)	5684 (15277)	3369 (9278)	2592 (7920)
Amorphous	717 (2102)	770 (3432)	3308 (7747)	1314 (3921)	2174 (3387)
Color fringe	3155 (4145)	1586 (8338)	7267 (21206)	1223 (1558)	3134 (7795)

Table 7 shows the Wilcoxon test for open meshwork LLP, and it was found that there were significant differences only when comparing the size of EC area between observer 1 and observer 4 ($p = 0.010$) and between observer 4 and the automatic system ($p = 0.020$).

Table 7. Wilcoxon test outcomes for open meshwork lipid layer pattern categorization. Pair wise comparisons were done between the amount of EC pixels categorized by two observers. In each comparison median of differences and level of statistical significance (p) are indicated. EC: “Erroneous categorization”, means those pixels that reference observer agreed with 0 observers or were marked only by the reference observer.

Pair wise comparisons. Open meshwork pattern categorization				
	Observer 1	Observer 2	Observer 3	Observer 4
Observer 1				
Observer 2	$p = 0.210$			
Observer 3	$p = 0.090$	$p = 0.210$		
Observer 4	$p = 0.090$	$p = 0.120$	$p = 0.010$	
Automatic system	$p = 0.670$	$p = 0.480$	$p = 0.120$	$p = 0.020$

4 Discussion

This study demonstrated an automatic tool, within the framework of *i*DEAS, to identify several LLP zones in a single patient image. In previous work [34], a preliminary study found that the automatic system (in terms of percentage of pixels that were in concordance with the observers) show similar categorization as done by other observers, especially for CO and OM LLPs, whereas W pattern show less percentage of coincidences [34]. In the present study, the automatic application was validated by comparing its performance against four experienced observers [23]. This was done to find out statistically how different is the categorization of LLP zones between the new application and the experienced observers and between the experienced observers themselves. As the material and method section explains, to facilitate the statistical analysis, the data were presented in two ways, (“perfect categorization”), which means pixels in concordance with all observers, and “erroneous categorization, which means pixels without concordance with any observer.

Firstly, it was evaluated whether each observer presented the same difficulty in categorizing each LLPs, and it was found true, because of the lack of differences between pixels both for EC and PC. This indicates consistency in the categorization done by the 5 observers along with all types of LLPs.

Secondly, categorizations of LLP zones were compared among the 5 observers, both as a whole and by each LLP. In this case, only EC was considered because, as was explained earlier in the results section, PC areas are the same for the 5 observers. In general, observer 3 classified worse than the remaining 4 observers (Tables 4 and 5) and the automatic system was classified worse only when comparing with observer 4 (observer 4 was the most conservative). However, these differences were found only for the OM pattern (Tables 6 and 7), so in the remaining lipid layer categories, there was a consistency among observers in the examination of the LLP areas.

According to the results obtained, we observe that the automatic application classifies the LLP zones that coincide with the one performed by experienced observers. Thus, the manual process done by experts can be automated with the benefits of being unaffected by subjective factors. This new software clearly improves the previous automatic application that was designed to categorize the whole pattern [33]. However, there is still large room for improvement on the processing time needed to generate the output image (10 minutes on average). Consequently, our future research will involve developing an optimized version whose processing time makes it useful in any clinical routine.

The concordance of the evaluations done by the four experienced observers provided us with a set of images that permit enhancing the descriptions of the LLPs (Figs 6-10 and Table 3), to minimize the variability of subjective classification. Descriptions of LLPs in this study are based on Guillon’s basic categories [20], though we have expanded these descriptions to provide as many details as possible derived from the experience of all the observers involved in this study. In effect, for this project, we have so far examined 680 videos and about 2000 images.

To better understand the description of the LLPs, we provide four images of each LLP (Figs 6 to 10), showing zones similarly outlined by 4 experienced observers who were blind to the pattern or the interpretations done by the other 3 observers. Each observer marked the zone that he/she differentiated as the given LLP in 50 images. Using the *i*DEAS application, the classifications of all the observers were compiled to give the marked zones similarly classified by the four observers. These sets of images offer clear examples of the main LLPs along with their detailed descriptions.

Although five main LLP categories are usually defined, transitions between patterns may be observed. In fact, several authors have used a more sensitive classification scheme than of Guillon including inter-categories.[43,44]. Isenberg *et al* [44] reported up to ten grades of LLP. Sometimes, it is difficult to classify an LLP because its characteristics are common to two pattern types. In this sense, observers were instructed in the presence of "intermediate LLPs" to help them correctly categorize the patterns (see appendix).

As LLP is based on interference phenomena formed by the beam reflected from the air-lipid tear film interface and the beam reflected from the lipid-aqueous tear film interface (Fig 1). Interference patterns can be visible because these two beams originate from the same point of the single light source, and the lipid layer is thin enough to guarantee that both beams satisfy the requirement of coherence. LLT can be extrapolated from LLPs, which is a useful parameter because there is some evidence that tear film is affected by LLT [45]. Guillon found that thicker LLPs correlated with better tear film stability and proposed a scheme of 5 main LLP categories that represented different LLT [45]. In Guillon's scheme, OM and CM were related to thickness of 15-30 nm, W was within 50-70 nm, AM indicates a lipid layer of 80 - 90 nm and CO refers to the thickest layer within 90-180 nm [20]. It can be noted that as OM and CM lipid layer patterns were related to the same LLT, so they were previously grouped in the same classification [46]. But, as Guillon stated, the main difference between the two mesh patterns is only the way the lipid layer is spread over the cornea [20], which makes very difficult to distinguish between OM and CM. On the other hand, different thicknesses for OM (with values between 10-20 nm) and CM (with values between 20-40 nm) patterns have been previously reported by Isenberg *et al* [44]. From a clinical point of view, both meshwork patterns should be distinguished, because the boundary between OM and CM represents the limit between abnormal LLP (OM) and "acceptable" pattern (CM) [20].

As an interferential phenomenon, the LLPs are related to colours appearance, and some authors only addressed the colours of patterns [25,28]. The authors considered that the best way to address the LLPs is by doing an analysis based on both texture and colour. However, the lipidic reflection does not always show a CO pattern. The observation of a colourless pattern (grey colour) is because lipid layer thickness is below the minimum thickness to produce interference fringes. Korb established the LLT that corresponded to each colour [25]. In Table 8, we show Guillon's scheme [20],

Table 8. Correspondence of thickness (nm) between Lipid layer pattern classification published by Guillon [17] and Isenberg *et al* [44] with Korb's classification based on color [21]. Note that shading cells indicate lack of thickness correspondence between classifications.

Guillon classification (LLP)	Korb classification (color)	Isenberg et al classification (lipid layer pattern)
		Open Meshwork (10-20 nm)
Open Meshwork (13 -50 nm)		Closed Meshwork (20-40 nm)
Closed Meshwork (13-50 nm)	Grey to white (30-60 nm)	
Wave (50-70 nm)		Wave (50-70 nm)
	Grey/yellow (75 nm)	
Amorphous (80-90 nm)	Yellow (90 nm)	Amorphous (80-90 nm)
	Yellow/brown (105 nm)	
	Brown/yellow (120 nm)	
Color Fringe (90-180 nm)	Brown (135 nm)	Color Fringe (> 100 nm)
	Brown/blue (150 nm)	
	Blue/brown (165 nm)	
	Blue (180 nm)	

the classification published by Isenberg *et al* [44] and their correspondence with Korb's classification based on colour.[25]. From those classifications it can be seen that thinner LLPs (from OM to W) showed a grey background, and yellow colour begins to appreciate in the transition of W and A patterns.

In our experience [33], we have noted that the thicker the lipid layer, the more marked appear the details of the pattern. Thus, as the lipid layer gets thicker, the pattern produced goes through the following stages: almost no details on a dark background (OM); changing to visible dark streaks on an ever-brighter grey background followed by the merging of streaks to form large zig-zags (CM); until they thin out, and give rise to the flow wave pattern (W); the grey background then turns yellowish until waves disappear to give the amorphous pattern (AM); and finally on this yellow background, appear the first brown/blue colours (CO). We hope the wide LLP image database that we present here [37], could aid the observers in the LLP categorization.

5 Conclusion

The results of this study show that the automatic application included in the framework *iDEAS* is able to categorize LLP zones as done by experienced optometrists. This device offers a clear benefit in categorizing the heterogeneity of the LLP without being affected by subjective factors.

References

1. Craig J P, Nichols K K, Akpek E K, Caffery B, Dua H S, Joo CK, Liu Z, Nelson J D, Nichols J J, Tsubota K, Stapleton F, TFOS DEWS II Definition and Classification Report, *Ocul Surf*, 15(2017)276–83.
2. Khanal S, Tomlinson A, McFadyen A, Diaper C, Ramaesh K, Dry eye diagnosis, *Invest Ophthalmol Vis Sci*, 1407–1414.
3. Nichols K K, Nichols J J, Mitchell G L, The lack of association between signs and symptoms in patients with dry eye disease, *Cornea*, 23(2004)762–770.
4. Geerling G, Tauber J, Baudouin C, Goto E, Matsumoto Y, O'Brien T, Rolando M, Tsubota K, Nichols K K, The international workshop on meibomian gland dysfunction: report of the subcommittee on management and treatment of meibomian gland dysfunction. *Invest Ophthalmol Vis Sci*, 52(2011)2050–2064.
5. Tomlinson A, Blades K J, Pearce E I, What does the phenol red thread test actually measure? *Optom Vis Sci*, 78(2001)142–146.
6. Wolffsohn J S, Arita R, Chalmers R, Djalilian A, Dogru M, Dumbleton K, Gupta P K, Karpecki P, Lazreg S. TFOS DEWS II Diagnostic Methodology report, *Ocul Surf*, 15(2017)539–574.
7. Wolffsohn J S, Purslow C, Clinical monitoring of ocular physiology using digital image analysis, *Cont Lens Anterior Eye*, 26(2003)27–35.
8. Fieguth P, Simpson T. Automated measurement of bulbar redness, *Invest Ophthalmol Vis Sci*, 43(2002)340–347.
9. Ramos L, Barreira N, Mosquera A, Penedo M G, Yebra-Pimentel E, Garcia-Resua C. Analysis of parameters for the automatic computation of the tear film break-up time test based on CCLRU standards, *Comput Methods Programs Biomed*, 113(2014)715–724.
10. Pult H, Riede-Pult B, Comparison of subjective grading and objective assessment in meibography, *Cont Lens Anterior Eye*, 36(2013)22–27.
11. Pena-Verdeal H, Ramos L, Garcia-Queiruga J, Garcia-Resua C, Giraldez M J, Yebra-Pimentel E, Validation of a New Software Application for Tear Breakup Measurement, *Optom Vis Sci*, 99(2022)159–166.
12. Ramos L, Barreira N, Pena-Verdeal H, Giraldez M J, Automatic assessment of tear film break-up dynamics, *Stud Health Technol Inform*, 207(2014)173–182.
13. Sanchez Brea M L, Barreira Rodriguez N, Mosquera Gonzalez A, Evans K, Pena-Verdeal H, Defining the Optimal Region of Interest for Hyperemia Grading in the Bulbar Conjunctiva, *Comput Math Methods Med*, 2016(2016)3695014; doi.org/10.1155/2016/3695014.
14. Nichols K K, The international workshop on meibomian gland dysfunction: introduction, *Invest Ophthalmol Vis Sci*, 52(2011)1917–1921.

15. Nelson J D, Shimazaki J, Benitez-del-Castillo J M, Craig J P, McCulley J P, Den S, Foulks G N, The international workshop on meibomian gland dysfunction: report of the definition and classification subcommittee. *Invest Ophthalmol Vis Sci*, 52(2011)1930–1937.
16. Matsumoto Y, Dogru M, Goto E, Ishida R, Kojima T, Onguchi T, Yukiko Y, Jun S, Kazuo T, Efficacy of a new warm moist air device on tear functions of patients with simple meibomian gland dysfunction, *Cornea*, 25(2006)644–650.
17. Arita R, Itoh K, Maeda S, Maeda K, Furuta A, Fukuoka S, Tomidokoro A, Amano S, Proposed diagnostic criteria for obstructive meibomian gland dysfunction, *Ophthalmology*, 116(2009)2058-2063 e1.
18. King-Smith P E, Ramamoorthy P, Braun R J, Nichols J J, Tear film images and breakup analyzed using fluorescent quenching, *Invest Ophthalmol Vis Sci*, 54(2013)6003–6011.
19. Peng C C, Cerretani C, Braun R J, Radke C J, Evaporation-driven instability of the precorneal tear film. Advances in colloid and interface, *Science*, 206(2014)250–264.
20. Guillon J P, Non-invasive Tearscope Plus routine for contact lens fitting, *Contact Lens & Anterior Eye* (Supplement), 21(1998)S31–S40.
21. Rolando M, Valente C, Barabino S. New test to quantify lipid layer behavior in healthy subjects and patients with keratoconjunctivitis sicca, *Cornea*, 27(2008)866–870.
22. Giraldez M J, Naro S A, Resua C G. A preliminary investigation into the relationship between ocular surface temperature and lipid layer thickness, *Contact Lens & Anterior Eye*, 32(2009)177–180.
23. Garcia-Resua C, Pena-Verdeal H, Minones M, Giraldez MJ, Yebra-Pimentel E. Interobserver and intraobserver repeatability of lipid layer pattern evaluation by two experienced observers, *Contact Lens & Anterior Eye, J Br Contact Lens Assoc*, 37(2014)431–437.
24. Guillon J P, Abnormal lipid layers. Observation, differential diagnosis, and classification, *Adv Exp Med Biol*, 438(1998)309–313.
25. Korb D R (ed), The tear film-its role today and in the future. In: The tear film, structure, function and clinical evaluation, (Butterworth-Heinemann), 2002, pp 126-192.
26. Nichols J J, Nichols K K, Puent B, Saracino M, Mitchell G L, Evaluation of tear film interference patterns and measures of tear break-up time, *Optom Vis Sci*, 79(2002)363–369.
27. King-Smith P E, Fink B A, Fogt N. Three interferometric methods for measuring the thickness of layers of the tear film, *Optom Vis Sci*, 76(1999)19–32.
28. Goto E, Dogru M, Kojima T, Tsubota K. Computer-synthesis of an interference color chart of human tear lipid layer, by a colorimetric approach, *Invest Ophthalmol Vis Sci*, 44(2003)4693–4697.
29. Garcia-Marques J V, Talens-Estarellas C, Garcia-Lazaro S, Cervino A, Validation of a new objective method to assess lipid layer thickness without the need of an interferometer, *Graefes Arch Clin Exp Ophthalmol*, 260(2022)655–676.
30. Ting D S W, Tan T E, Lim C C T, Development and Validation of a Deep Learning System for Detection of Active Pulmonary Tuberculosis on Chest Radiographs: Clinical and Technical Considerations, *Clin Infect Dis*, 69(2019)748–750.
31. Lakhani P, Sundaram B, Deep Learning at Chest Radiography: Automated Classification of Pulmonary Tuberculosis by Using Convolutional Neural Networks, *Radiology*, 284(2017)574–582.
32. Remeseiro B, Bolon-Canedo V, Peteiro-Barral D, Alonso-Betanzos A, Guijarro-Berdinas B, Mosquera A, Penedo M, Sánchez-Marroño N, A methodology for improving tear film lipid layer classification, *IEEE J Biomed Health Inform*, 18(2014)1485–1493.
33. Garcia-Resua C, Giraldez Fernandez M J, Gonzalez Penedo M F, Calvo D, Penas M, Yebra-Pimentel E, New software application for clarifying tear film lipid layer patterns, *Cornea*, 32(2013)538–546.
34. Remeseiro B, Barreira N, Garcia-Resua C, Lira M, Giraldez M J, Yebra-Pimentel E, Penedo M, iDEAS: A web-based system for dry eye assessment, *Comput Methods Programs Biomed*, 130(2016)186–197.
35. Hecht E, Optics. 4th edn, (Addison-Wesley, San Francisco), 2002.
36. Guillon J P, Guillon M, The role of tears in contact lens performance and its measurement, In: Montague R, Guillon M, (eds), Contact lens practice, (Chapman and Hall Medical, London), 1994, pp 453–483.
37. Aydogdu S, Ertekin K, Suslu A, Ozdemir M, Celik E, Cocen U, Optical CO₂ sensing with ionic liquid doped electrospun nanofibers, *J Fluoresc*, 21(2011)607–613.

38. Remeseiro B, Penas M, Mosquera A, Novo J, Penedo M G, Yebra-Pimentel E, Statistical comparison of classifiers applied to the interferential tear film lipid layer automatic classification, *Comput Math Methods Med*, 2012(2012)207315; doi.org/10.1155/2012/207315.
39. Remeseiro B, Penas M, Barreira N, Mosquera A, Novo J, Garcia-Resua C. Automatic classification of the interferential tear film lipid layer using colour texture analysis, *Comput Methods Programs Biomed*, 111(2013)93–103.
40. Remeseiro B, Ramos L, Barreira N, Mosquera A, Yebra-Pimentel E, Colour texture segmentation of tear film lipid layer images. In: Moreno-Díaz R, Pichler F, Quesada-Arencibia A (eds), *Computer Aided Systems Theory, Lecture Notes in Computer Science*, (Springer, Berlin), 2013, pp140–147.
41. McLaren K. The development of the CIE 1976 (L*a*b) uniform colour-space and colour-difference formula, *J Soc Dyers Colourists*, 92(1976)338–341.
42. Haralick R M, Shanmugam K, Dinstein I, Textural features for image classification, *IEEE Transactions on Systems, Man and Cybernetics*, SMC-3(1973)610–621.
43. Maissa C, Guillon M, Tear film dynamics and lipid layer characteristics--effect of age and gender, *Cont Lens Anterior Eye*, 33(2010)176–182.
44. Isenberg S J, Signore M D, Chen A, Wei J, Guillon J P, The lipid layer and stability of the preocular tear film in newborns and infants, *Ophthalmology*, 110(2003)1408–1411.
45. Foulks G N, The correlation between the tear film lipid layer and dry eye disease, *Surv Ophthalmol*, 52(2007)369–374.
46. Patel S, Wallace I, Tear meniscus height, lower punctum lacrimale, and the tear lipid layer in normal aging, *Optom Vis Sci*, 83(2006)731–739.

[Received: 25.03.2023; revised recd: 29.04.2023; accepted: 30.04.2023]

APPENDIX: Guide to subjective categorization of LLPs

Lipid layer pattern (LLP) interpretation to LLP categorization was based on Guillon's scheme [20]. Three intermediate LLPs were defined to avoid possible misinterpretations and enhance the sensitivity of the technique: an intermediate pattern between OM and CM (called OMCM), one between CM and W (CMW) and a third between W and AM (WAM). Example images as well as description of both standard and intermediate LLPs, are shown in Figs 11-18.

1 Open meshwork pattern (OM)

This is a grey, marble-like open meshwork of very spaced black streaks, which are hardly visible on a slightly shiny grey background (Fig 11).



Fig 11. Open meshwork pattern (OM). A gray, marble-like open meshwork of very spaced black streaks, which are hardly visible on a slightly shiny gray background. Note the iris can be seen through the pattern.

2 Intermediate open-closed meshwork pattern (OMCM)

As the lipid layer thickens, the meshwork becomes more compact resulting in a transition pattern between the open and closed meshwork patterns (OMCM). It is difficult to differentiate this pattern as an open or closed meshwork. It is similar to OM, though dark streaks are less spaced, revealing a slightly more visible and detailed pattern. This pattern, however, lacks the levels of detail of the next LLP (Fig 12).



Fig 12. Intermediate open-closed meshwork pattern (OMCM). Dark streaks are less spaced than in the OM, revealing a slightly more visible and detailed pattern. This pattern lacks the level of detail of the next LLP.

3 Closed meshwork pattern (CM)

It is similar to marbled gray pattern, but streaks are more compact and form a tightly-closed mesh. Sometimes streaks appear as very open, thick zig-zags (Fig 13).

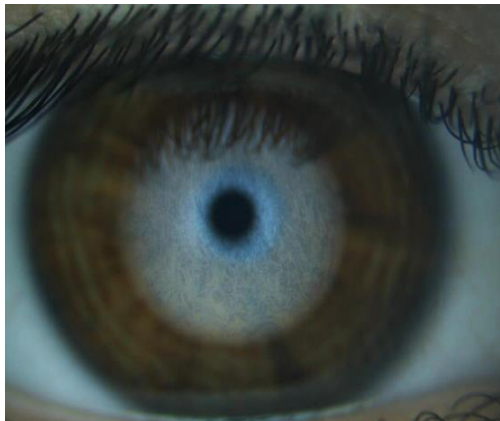


Fig 13. Closed meshwork pattern (CM). Streaks are more compact and form a tightly-closed meshwork pattern to give a better defined picture.

4 Intermediate closed meshwork-wave pattern (CMW)

As LLT continues to increase, we see that the pattern becomes more flowing or continuous between the closed meshwork and wave patterns. There are two alternative characteristic features of the intermediate pattern: streaks can be observed both as thick wavy lines or as thin zig-zagging lines (Fig 14).

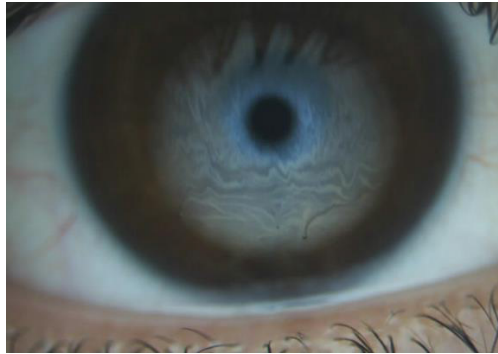


Fig 14. Intermediate closed meshwork-wave pattern (CMW). Streaks appearing as thick wavy lines (white arrows).

5 Wave/flow pattern (W)

In this pattern, the streaks appear as thin waves (**Fig 15**).

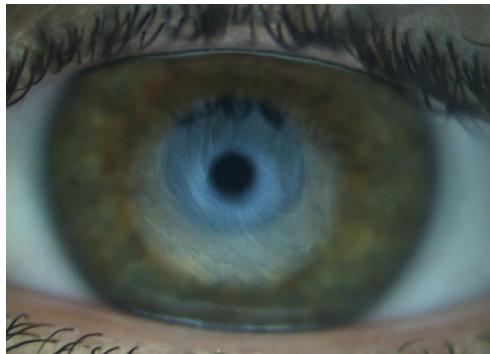


Fig 15. Wave pattern. Streaks appear as thin waves (W).

6 Intermediate wave-amorphous pattern (WAM)

The lipid layer becomes increasingly thicker, and a yellowish background colour (as in the amorphous pattern) appears. Streaks appear as in the wave pattern, but the background is yellowish rather than grey. This yellowish colour indicates a zone of a thicker lipid layer (**Fig 16**).



Fig 16. Intermediate wave-amorphous pattern (WAM). Streaks appear as waves but this time on a yellowish background. This yellowish color indicates a zone of thicker lipid layer.

7 Amorphous pattern (AM)

This is a bright white/yellowish homogenous background with no streaks (Fig 17).



Fig 17. Amorphous pattern (AM). A bright white/yellowish homogenous background with no streaks.

8 Colour fringe pattern (CO)

Thick lipid layers with high lipid contents produce a colour fringe pattern. This pattern consists of interference colours, yellow, brown, blue and purple (Fig 18).



Fig 18. Color fringe pattern (CO). This pattern consists of interference colors, yellow, brown, blue and purple.



Professor Dr Maria J Giraldez is currently Head of the Optics and Optometry Faculty at Santiago de Compostela University (USC), Spain. She received her Optics Degree and Optics and Optometry Degree from Complutense University, Madrid and from Granada University (Spain) in 1990 and 1994, respectively. She pursued her Master degree at USC, and in 2010 she successfully completed her Ph D in the Optics, Optometry and Vision program at Complutense University, Madrid. Since 1992 she has been Professor of the Optics and Optometry Faculty at Santiago de Compostela University. She is member of the USC Research Group GI-2092- Optometry, and of the Health Research Institute of Santiago de Compostela (IDIS). With around 63 publications, she is Professor and Thesis Director of the Doctoral Program in Molecular Medicine (Research Line: Techniques applied to biomedical research) of the International Doctoral School of the USC. María J Giráldez carried out different research stays in Berkeley where she worked in the research line Hyperacuity: types and clinical applications, directed by Professor Jay M Enoch.



Dr Carlos Garcia-Resua is a lecturer and researcher in the Area of Optometry at the University of Santiago de Compostela (Spain). He was graduated with honors in Optics and Optometry (Santiago de Compostela University) in 1999, and then obtained his M Sc. His research was conducted on myopia, intraocular pressure measurement, and currently is focused on tear film. In 2016 he completed his Ph D in the Molecular Medicine program of the University of Santiago de Compostela with a thesis on Dry Eye Disease diagnosis, achieving the highest mark. He published around fifty peer-reviewed articles, one book, five book chapters and 98 presentations in international meetings. In 2016, he became Assistant Professor, and since 2021 he is Permanent Professor of the University of Santiago de Compostela.



Dr Hugo Pena Verdeal, a native of Galicia, is a lecturer and researcher in the field of Optometry at the University of Santiago de Compostela in Spain. He obtained his Optics and Optometry degree and pursued Master's in Neuroscience Research at the University of Santiago de Compostela. In 2016, he successfully completed his Ph D in the Molecular Medicine Program at the same university, earning the highest distinction for his thesis on the diagnosis of Dry Eye Disease. Dr Hugo Pena Verdeal has published approximately 30 journal articles and book chapters, in addition to presenting over 70 research findings at international conferences. Since 2017, he has been actively involved in teaching clinical subjects in the Area of Optometry, specifically at the Optometry Clinic.



Jacobo Garcia-Queiruga is an assistant lecturer in the Area of Optometry at the University of Santiago de Compostela (Spain). He holds a degree in Optics and Optometry (2016) and a M Sc in Research in Vision Science (2017), both from the University of Santiago de Compostela. In 2017, he started his Ph D studies in the field of ocular surface and Dry Eye, focusing on Evaporative Dry Eye and Meibomian Gland Dysfunction. He became assistant lecturer in 2019. He has published twelve papers in JCR indexed journals and presented over 30 communications at international conferences. He teaches contactology and optometry fundamentals in the Optics and Optometry degree, and dry eye and ocular discomfort in the Master of Optometry.



Professor Dr Eva Yebra-Pimentel is currently Director of the Clinic of Optometry (Santiago de Compostela University, Spain). She was Dean of the Optics and Optometry Faculty from 2001 to 2010. She received her Pharmacy Degree,

Optics and Optometry Degree and Ph D (1993) at Santiago de Compostela University (USC). Since 1990, she has been Professor of Optometry at the Optics and Optometry Faculty (USC).

She leads the USC Research Group GI-2092- Optometry and is member of the Health Research Institute of Santiago de Compostela (IDIS). With more than 90 publications, she is Professor and Thesis Director of the Doctoral Program in Molecular Medicine (Research Line: Techniques applied to biomedical research) of the International Doctoral School of the USC. Eva Yebra-Pimentel carried out different research stays in Berkeley where she worked in the research line Hyperacuity: types and clinical applications, directed by Professor Jay M Enoch.